PAPER

Check for updates

Integration of Ni/NiO nanoparticles and a microfluidic ELISA chip to generate a sensing platform for *Streptococcus pneumoniae* detection†

Chang-Ching Weng,[a] Chien-Yu Chao,[b] She-Ting Wu,[b] Ping-Hsien Tsou, [iD][c] Wei-Tin Chen, [iD] *[d] Bor-Ran Li [iD] *[bef] and Yaw-Kuen Li [iD] *[af]

Enzyme-linked immunosorbent assays (ELISAs) are tests that uses antibody recognition and enzyme catalytic activity to identify a substance, and they have been widely used as a diagnostic tool in the clinic. However, performing an ELISA requires various liquid handling steps and long binding times. To solve this problem, we developed a magnetic microfluidic ELISA system (MMF-ELISA). Integration with nickel magnetic nanoparticles can streamline the ELISA process in a fully automated manner for *Streptococcus pneumoniae* detection. First, we synthesized paramagnetic surface-oxidized nickel nanoparticles (Ni/NiO NPs) to carry protein G. Then, we assembled a SUM290 (UlaG)-specific antibody on protein G. Finally, we integrated the NPs on a microfluidics chip for *S. pneumoniae* detection. The chip contains three different layers to trap the solutions; the bottom layer SiO_2 is patterned on hydrophobic polymers and integrated with the middle layer PDMS and the top layer PMMA. With Arduino and motor IC, we developed an automated platform for *S. pneumoniae* detection. Microfluidic ELISAs can reduce the manual handling and operation time. Furthermore, the developed system can be extended to multiple areas for ELISA-related assays. This economical, rapid and portable system may become a promising platform for sensing *S. pneumoniae* in clinical applications.

1. Introduction

Streptococcus pneumoniae causes various infectious diseases, primarily sepsis, pneumonia, and meningitis.[1–3] More than 400 million individuals are infected with *S. pneumoniae* every year, and more than one million mortalities have been reported. The current gold standard to detect *S. pneumoniae* is conventional bacterial culture, which still relies on bacterial isolation from specimens and time-consuming culture on specific media. The alternative methods are the PCR-based nucleic acid amplification test (NAAT)[4] and immunochromatography assay (ICA)[5] to detect urinary antigens (for instance, BinaxNOW®). Although these methods are

rapid and accurate, NAATs are costly and require specific equipment. The ICA BinaxNOW®[6] is a good example of a point-of-care (POC) assay that is rapidly and effectively used to diagnose systemic pneumococcal infections105. However, the urinary antigen test for *S. pneumoniae* has a shelf life of only a month; hence, the chances of a misdiagnosis are high, and there is a limited sensitivity due to its method of developing signals.

Point-of-care (POC) diagnosis refers to the rapid and effective diagnosis and analysis of patients in the laboratory or clinical setting without the need for large or expensive instruments using a portable, convenient, and inexpensive device.[7–10] This technology can be used for specific cells or molecules, is easy to use and yields results in a few minutes, and the tests previously requiring professionals can now be performed by patients and civilians themselves. Advancements in diagnostic equipment have yielded related portable, handheld instruments, or reagent-based assays, which have evolved from providing treatment and predicting disease progression to personalized and preventive medicine. Driven by medical needs, scientific and technological advancements, and reduced medical costs, POC systems have gradually been enhanced, yielding rapid results and providing more resources to diagnose diseases and administer appropriate treatment while providing patient care. This technology involves products including biosensing systems, microsystems, and low-cost imaging technology. With the aging of the population and the improvement in health awareness,[11–13] *in vitro* diagnostic methods

[a]*Department of Applied Chemistry, College of Science, Yang Ming Chiao Tung University, Hsinchu, Taiwan*

[b]*Institute of Biomedical Engineering, College of Electrical and Computer Engineering, Yang Ming Chiao Tung University, Hsinchu, Taiwan. E-mail: liborran@g2.nctu.edu.tw*

[c]*Department of Internal Medicine, National Taiwan University Hospital, Hsin-Chu Branch, Hsinchu, Taiwan*

[d]*Center for Condensed Matter Sciences, Center of Atomic Initiative for New Materials, National Taiwan University, Taipei, Taiwan. E-mail: weitinchen@ntu.edu.tw*

[e]*Department of Eectrical and Computer Engineering, College of Electrical and Computer Engineering, Yang Ming Chiao Tung University, Hsinchu, Taiwan*

[f]*Center for Emergent Functional Matter Science, Yang Ming Chiao Tung University, Hsinchu, Taiwan. E-mail: nctuykl@g2.nctu.edu.tw*

† Electronic supplementary information (ESI) available. See DOI: 10.1039/d1ra04631d

have developed rapidly in recent years in the medical equipment industry; however, they have numerous issues, including those related to sensitivity and specificity, the preprocessing of complex samples, the detection of trace components, *etc.*[10,14–16] The advantages of using magnetic nanoparticles (MNPs) are that they can improve the sensitivity and specificity of the detected samples, and they are widely used in biomedical separation methods.[17–19] ELISA is based on the antigen–antibody interaction, and a positive result is obtained upon enzymatic coloration.[19] This method is extensively used to detect biological material; however, the technical limitations of ELISA include the requirement of a liquid system and long reaction time, which thereby limits the scope for method enhancement.[20–22]

In this study, a magnetic microfluidic ELISA system (MMF-ELISA) was designed to allow for rapid ELISA systems (Fig. 1). Ni/NiO nanoparticles (Ni/NiO NPs) were initially generated *via* chemical reduction as a carrier for histidine-tagged Gβ1 protein and further conjugated with an antibody against SMU290, an *S. pneumoniae* surface protein, and microbial detection was carried out on a microfluidic chip. A trichloro-($1H,1H,2H,2H$-perfluorooctyl)-fluorane fluoroalkyl silane (FAS) coating was applied to the microchannel chip, and mineral oil was mixed in the hydrophobic region of the FAS coating to demarcate the hydrophilic detection zone. In the hydrophilic region of the glass surface, which did not contain an FAS coating, various detection solutions were mixed with Ni/NiO NPs, which were manipulated under a magnetic field to cross the hydrophilic/hydrophobic interface necessary for multistep biochemical reactions. This approach was applied for automated ELISA to reduce errors in artificial displacement and to increase the sensitivity of detection. This system can be used for immunoassays in remote areas and has potential clinical applications.

2. Materials and methods

2.1 Materials

Nickel(ɪɪ) chloride, CAS 7718-54-9, 98% (Sigma-Aldrich, USA), sodium borohydride, CAS 16940-66-2, 98% (Alfa Aesar, USA),

polyvinylpyrrolidone (PVP), CAS 9003-39-8 (Sigma-Aldrich), green fluorescent protein (GFP-12xHis) with histamine tag (Huang Yuting), *Streptococcus pneumoniae* ATCC 49136 (Master Zhang Jiayu), *Streptococcus mutans* ATCC 25175 (Master Zhang Jiayu), *Streptococcus pyogenes* ATCC 12344 (Master Zhang Jiayu), Rabbit anti-SMU290 antibody (Zhang Jiayu), SureBlueᵀᴹ TMBMicrowell peroxidase substrate (1-Component) (No. 52-00-00, KPL), Ni Sepharose 6 Fast Flow (No. 17-5318-01, GE Healthcare Life Sciences, USA), Peroxidase-conjugated Affini-Pure goat anti-rabbit IgG (H + L) (No. 111-035-003, Jackson ImmunoResearch, USA), AffiniPure goat anti-rabbit IgG (H + L) (No. 111-005-003, Jackson ImmunoResearch), ChromPure mouse IgG, whole molecule (No. 015-000-003, Jackson ImmunoResearch), *Streptococcus pneumoniae* antibody: anti-SMU290 antibody from rabbit (Zhang Jiayu), pRSET_Gβ1 *Escherichia coli* (*E. coli*) BL21 (DE3) colony (Huang Yuting Xueyu), pRSET_SMU290 *E. coli* BL21 (DE3) colony (Zhang Jiayu), reagents for the culture solution (Zymeset, Sigma, Merck, Germany), and reagents for the buffer (Sigma, Lianhe Company, USA), FAS (Evonik, Germany) were used as precursors without any further purification. Argon was used as the carrier gas.

2.2 Surface modification of the FAS-interlayer films

Surface modification was performed using an atmospheric plasma jet (Fig. S1†).[23,24] The glass slide was soaked in isopropyl alcohol and ultrasonicated for 10 min, followed by removal of the glass surface with Clean Dry Air (CDA) plasma. Glasses were first clasped by a designed template mask. A pattern was generated using SolidWorks software. A laser cutting machine at 20 mm s⁻¹ and 60 W was used to fabricate the mask. A cardboard stencil mask was used to transfer the pattern to the glass. CDA was used as the main gas to generate plasma, and AC power was used as the plasma power supply fixed at 400 W with a fixed frequency of 35 kHz for all experiments. FAS was used as a precursor for the deposition of interlayer films, which were evaporated and injected into the atmospheric plasma jet at the end of the nozzle with argon as the carrier gas. The carrier gas
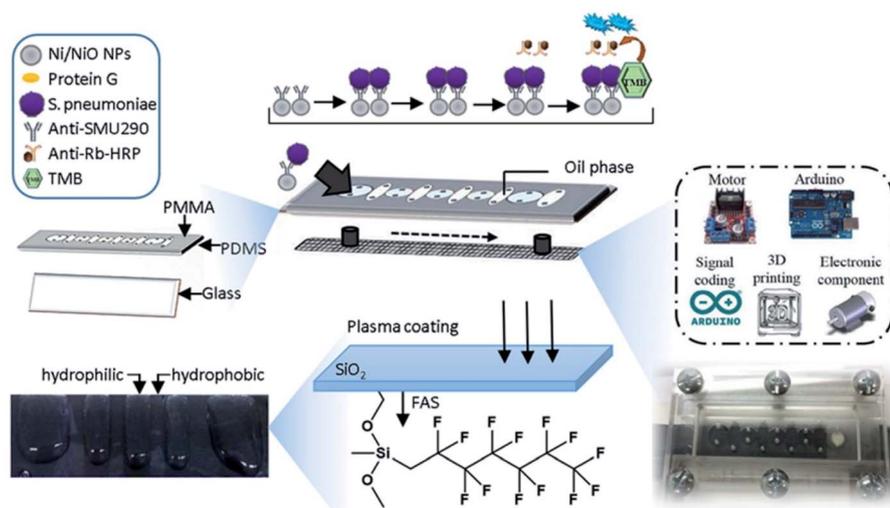

Fig. 1 Illustration of the magnetic microfluidic ELISA system (MMF–ELISA).

flow rate of FAS was optimized to 300 standard cubic centimeters per minute (sccm). The gap between the nozzle and substrate was 35 mm. The plasma jet traveled back and forth over the sample at a speed of 125 mm s^{-1}. The entire coating process took approximately 10 min. A warm water bath (60 °C) was used for the precursor. Before the experiment, any residual outside air in the precursor tube was eliminated, passing the carrier gas in the tank for 1 min. A deposit-free nozzle was required to prevent cross-reactivity with other impurities on the nozzle when the plasma was generated. Before coating, the air plasma stood for 3 min, and the electrode approached the working temperature. The parameters for the atmospheric pressure plasma jet treatment are summarized in Table 1.

2.3 Construction of the microfluid ELISA chip

The microfluidic chip designed herein comprises three layers, and the middle polydimethylsiloxane (PDMS) layer comprises an alternating arrangement of five circles (radius, 3.5 mm) and five ellipses (13 mm × 4 mm) in a line. The PDMS thickness was 0.8 mm, and the bottom glass (SiO$_2$) layer had a design template to modify the hydrophobic interlayers through atmospheric plasma. Circular infusion holes (radius, 0.5 mm) were drilled in the upper PMMA layer. Finally, the three different layers entrapped the solution on hydrophobic films within the hydrophobic interlayers containing mineral oil (Fig. 2a). SolidWorks 3D drawing software was used to design the three-dimensional mold. The image was saved as an STL file and transmitted to the engraving system to engrave an acrylic block (30 mm × 80 mm) using suitable tools and parameters. Engraving was carried out in three steps (leveling, rough carving, and fine engraving) to yield the finished mold. Appropriate amounts of PDMS glue A and B were evenly mixed in a 10 : 1 ratio then added to fill the mold, and a vacuum dryer was applied for 2 min to eliminate air bubbles in the glue. Excess PDMS solvent was scraped off, and then the mold was baked in an oven at 80 °C for 40 min. After that, the designed PDMS film layer was removed from the mold, and had a size of 76 mm × 26 mm × 0.8 mm (Fig. 2b).

2.4 Purification and performance of the GB1 protein

In this experiment, the constructed pRSET_GB1 was transferred into *E. coli* BL21 (DE3) for protein expression. The performance of the pSET A expression vector system is mainly driven by the lacZ promoter, while IPTG (isopropyl β-D-1-thiogalactopyranoside) induces the translation of the target gene to overexpress the target protein. After culturing 500 ml of the bacterial solution, the bacteria were lysed, and the obtained intracellular crude extract was passed through a Ni column (10 ml Ni Sepharose 6 Fast Flow). The column was functionalized with a GB1 protein with His-tag and nickel ions (nickel ions) for
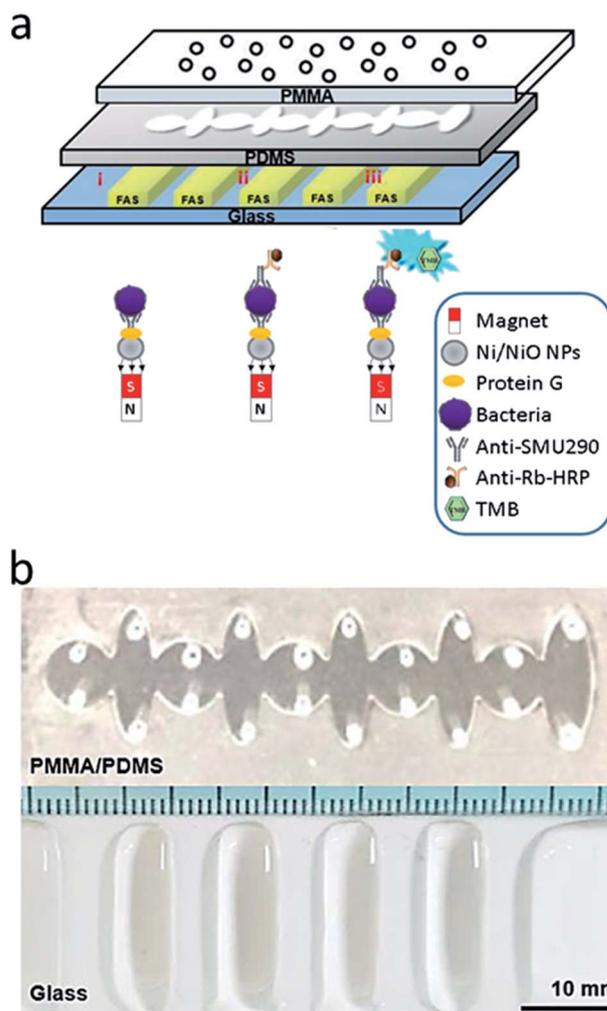

Fig. 2 Construction of the magnetic microfluidic ELISA system (MMF-ELISA). (a) Illustration of the working principle of the microfluidic ELISA approach. (b) Image of the microfluidic chip (the top region contains a combination of polymethylmethacrylate and polydimethylsiloxane, and the bottom region is glass).

purification. Elution was carried out using an imidazole (imidazole) salt gradient (5, 100, 300, 500 mM) to attain protein separation. This experiment was conducted with imidazole PBS at a flow rate of 2 ml min^{-1}. The buffer and flow washes were collected every 2 minutes, and seven elution fractions were collected for each imidazole concentration.

3. Results and discussions

3.1 Characterization of the FAS- modified surface

X-ray photoelectron spectroscopy revealed that the surface of the material contains fluorine (F), and it was confirmed that

Table 1 Parameters of the plasma treatment of FAS-modified ELISA chips

Precursor	Gap (mm)	Power (Watt)	Flow rates (sccm)	Scan speed (mm s^{-1})	Temperature (°C)	Scan times (times)
FAS	35	350	300	150	60	30

the application of FAS by atmospheric plasma can effectively modify the glass surface with fluorine to form a hydrophobic surface (Fig. 3a). After the substrate was coated with FAS, the surface energy decreased, and the water contact angle increased to 90°. After modification, the oil contact angle approached 80°. The structure of the FAS layer was disrupted *via* the generation of a small amount of oxygen-containing functional groups during plasma plating in the atmosphere. Nevertheless, the damaged FAS bore the weight of the oil at small volumes (5 μl; Fig. 3b). For a larger oil volume (20 μl), as in the present case, the disrupted FAS layer structure facilitated the passage of oil through the oxygen functional group that slowly penetrated the FAS film layer. As the FAS layer no longer completely isolated the substrate from the oil, the contact angle decreased to 20°. The oil is more likely to adhere to the FAS coating than to the untreated glass, thus the oil is patterned on the FAS-modified film. The different degrees of lipophilicity between the glass and the FAS film and the repulsive force allow the oil to be patterned on the FAS film.
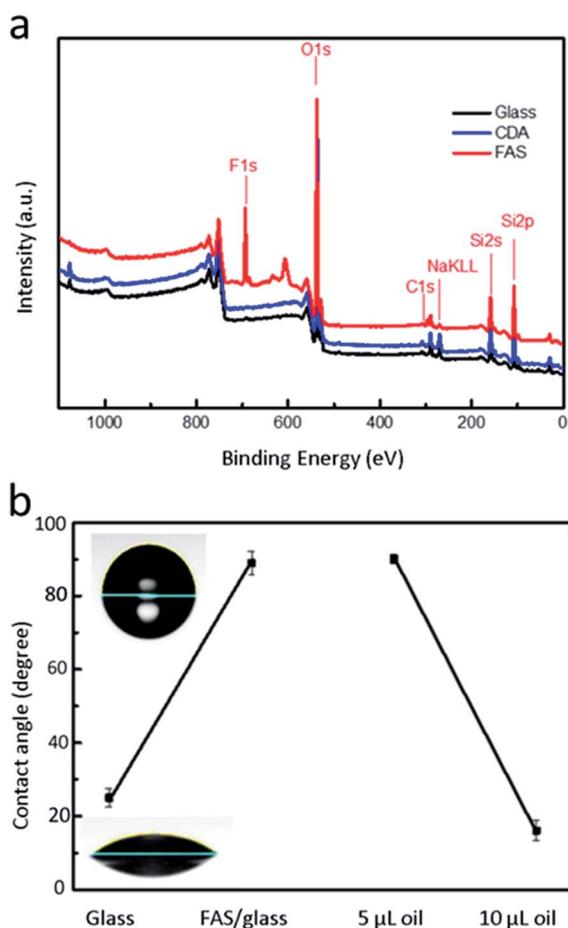
3.2 Characterization of the Ni/NiO NPs

Ni/NiO NPs were generated *via* chemical reduction at the annealing step at 400 °C. GFP with 12 His residues (GFP-12His) was used to bind to the Ni/NiO NPs.[25] Because of green fluorescence emitted by GFP, the beads binding to GFP also emitted green fluorescence. (Fig. 4a(i) and (ii)). Consequently, the Ni/NiO NPs displayed normal fluorescence. The GFP-12His-conjugated Ni/NiO NPs did not emit green fluorescence (Fig. 4a(iii) and (iv)). Green fluorescence was consistent with the position of the magnetic beads when viewed under white light, indicating that the experiment was successful with the His-tag. GFP was surface-modified on the Ni/NiO NPs. Similarly, other proteins with the same His-tag could be added. The surface of
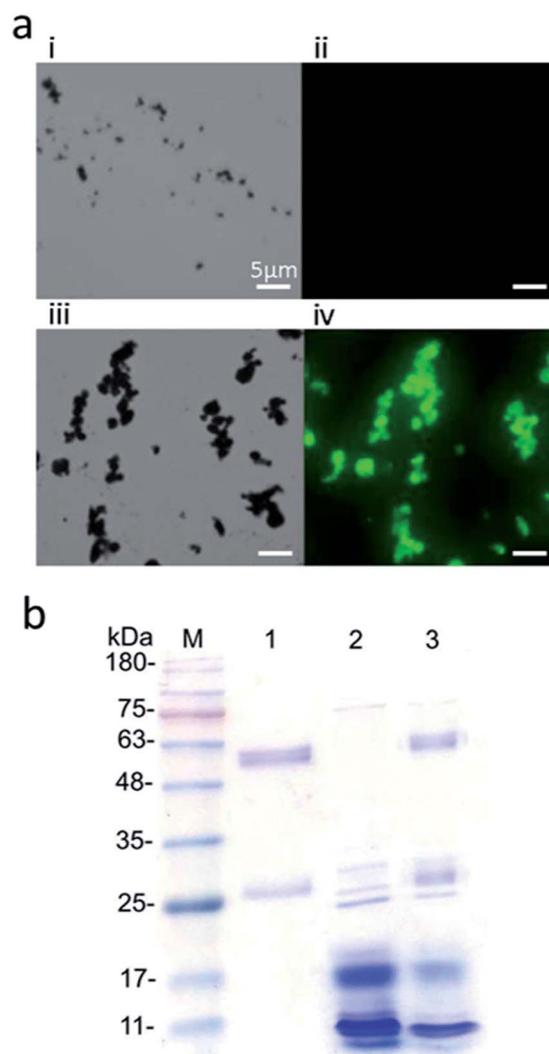

Fig. 4 (a) Imaging of the Ni/NiO nanoparticles stained with FITC-labeled GFP-12His. (i) A bright-field microscopic view of Ni/NiO nanoparticles (ii) excited at 488 nm. (iii) A bright view of Ni/NiO nanoparticles with GFP-12His (iv) excited at a wavelength of 488 nm with GFP-12His. (b) SDS-PAGE analysis of nickel nanoparticle (Ni/NiO NP)-conjugated protein G and anti-IgG. (1) Denatured anti-IgG heavy (50 kDa) and light (25 kDa) chains. (2) Ni/NiO NPs conjugate protein G (10 kDa). (3) Ni/NiO NPs conjugate protein G and anti-IgG.

Fig. 3 Characteristics of FAS-modified glass. (a) X-ray photoelectron spectroscopic analysis (glass, CDA, FAS). (b) Contact angles of droplets before and after surface modification. The contact angle of oil on the hydrophobic membrane with 5 μl and 20 μl oil.

the Ni/NiO NPs can be further modified for subsequent applications.

3.3 Conjugation of the Gβ1 protein to the anti-SMU290 antibody on the surface of the Ni/NiO NPs

One milligram of Ni/NiO NPs was uniformly shaken with 0.65 mg ml^{-1} GB1 protein for 1 h and washed three times with PBST (0.1% Tween-20) to eliminate proteins nonspecifically adsorbed on the surface of the magnetic beads. The same procedure was followed to configure another set of magnetic beads modified with Gβ1 protein, followed by shaking with 0.8 mg ml^{-1} mouse IgG for 1 h using PBST. After that, a discernible amount of denaturing dye was added, and the mixture was heated at 95 °C for 5 min for desorption of the protein modified on the magnetic beads. Electrophoresis was carried out to confirm the interactions between Ni/NiO NPs, Gβ1 proteins, and mouse IgGs. Fig. 4b shows the electropherogram of the Ni/NiO NPs with modified Gβ1 protein and mouse IgG. The Gβ1 protein bound and captured with mouse IgG *via* Ni/NiO NPs. Mouse IgG (150 kDa) was pyrolyzed to a heavy chain (50 kDa) and a light chain (light chain, 25 kDa). Consequently, the surface structure of the magnetic beads
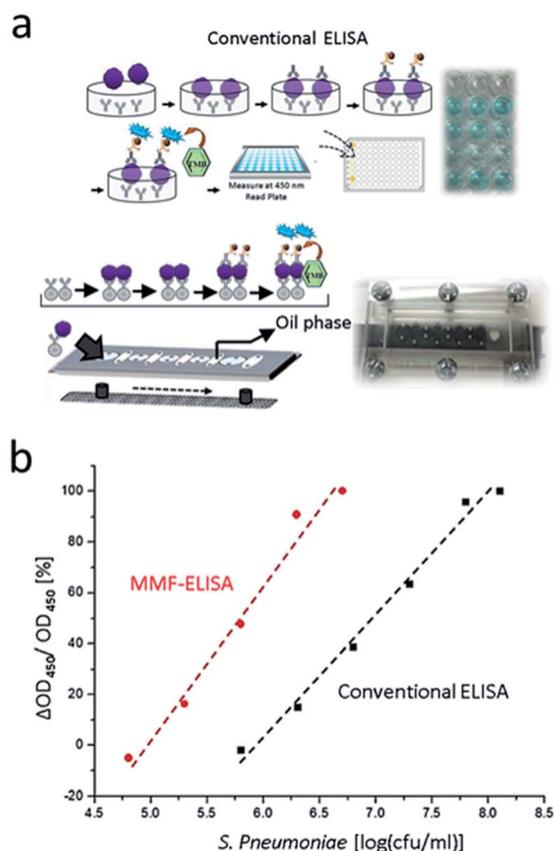

Fig. 5 (a) Illustration of the MMF-ELISA and conventional ELISA. (b) Comparison of the MMF-ELISA and conventional ELISA. The detection of *Streptococcus pneumoniae via* conventional ELISA (black) and with a microfluidic ELISA chip integrated with Ni/NiO magnetic nanoparticles (red).

caused nonspecific physical adsorption of the antibody, thereby potentially affecting the antigen–antibody reaction in the subsequent enzyme immunoassay. Therefore, the solution could be blocked with 5% skim milk powder to prevent nonspecific adherence of the antibody to the surface of the magnetic beads. The milk powder contains a large amount of casein, which does not participate in the reaction, thus filling the space on the magnetic beads and blocking the surface adsorption of the antibody. The major reason for using Ni/NiO particles is that the NiO layer can specifically bind histidine-tagged proteins without other modifications. Here, the protein Gβ1 domain was fused with histidine-tag to bind on the NiO surface, and Gβ1 provided the ability to binding the antibody on its Fc domain (Fig. S2†).

3.4 Detection of *S. pneumoniae*

A microfluidic enzyme immunoassay platform was established as shown in Fig. 5. Ni/NiO NPs were used for microfluidic ELISA, as opposed to conventional ELISA using a 96-well plastic plate coated with the antigen. The rubber disk interacts with the two-dimensional horizontal space, and the antigen and antibody solutions are mutually mixed *via* concentration-dependent diffusion, thus increasing the reaction time. The magnetic bead ELISA uses three-dimensional space to enhance the area of contact between the antigen and the solid carrier. Uniform mixing of the magnetic beads in the target solution not only improves contact efficiency but also facilitates their effective collection and dispersion in a magnetic field. The magnetic beads in the solution improve the reaction efficiency and shorten the overall reaction time. Anti-SMU290 antibody is a highly selective antibody reported in our previous studies (Fig. S3†). This experiment potentially modified the magnetic properties of the Gβ1 protein. Ni/NiO NPs initially reacted with 5% skim milk as a blocking solution to prevent the nonspecific adhesion of subsequent antibodies, followed by treatment with Gβ1. Anti-SMU290 interacted with the *S. pneumoniae* antigen at different concentrations (overexpression, OE). After blocking, the secondary antibody anti-rabbit IgG was added to ensure recognition junctions. *S. pneumoniae* was finally quantified through the color reaction resulting from the interaction between the HRP-labeled anti-rabbit IgG and TMB substrate. Fig. 5a shows the microfluidic ELISA using Ni/NiO NPs at different cellular densities of *S. pneumoniae*. This method can effectively detect *S. pneumoniae* with the surface protein SMU290 – *S. pn* (OE) and determine the detection limit (10^5–10^7 cfu ml^{-1}) of *S. pneumoniae*, which is lower than that of conventional ELISA. The results are shown in Fig. 5b, and they

Table 2 Comparison of the microfluidic ELISA chip and conventional ELISA

	Detection time (min)	Detection range (cfu ml^{-1})
This study	12	~10^5–10^7
Conventional method	30	~10^6–10^9

indicate that the application of magnetic nickel nanoparticles facilitates ELISA-based bacterial detection with an increased detection limit (Table 2).

4. Conclusions

In this study, a simple *S. pneumoniae* detection platform was established using modified Ni/NiO NPs as a solid carrier for a magnetic microfluidic ELISA system (MMF-ELISA). Rapid and effective detection was achieved through the combined use of the microfluidic ELISA chip and an automated control system. Ni/NiO NPs were integrated into the microfluidic ELISA chip with modified FAS-interlayered films. Consequently, the reaction time was reduced, and the sensitivity of the platform increased. Rapid and effective detection was achieved within 15 minutes and with a detection range of 10^5–10^7 cfu ml^{-1}, indicating that the application of Ni/NiO NPs facilitates ELISA-based microbial detection at an improved detection limit. Compared to conventional ELISA technology (pneumoniae), this new approach allows surfaces to be modified in a straightforward manner, enabling a cost-effective, rapid, and efficient biomedical sensing platform with a reduced need for human intervention. Although this microfluidic ELISA system take some advantage, it still has shortage of only 1 sample can be detected while the 96-well ELISA plate allow the detection of the large-scale samples in parallel. Thus, it still needs further improvements.

Conflicts of interest

There are no conflicts to declare.

Acknowledgements

References

1 C.-Y. Chang, H.-J. Lin, B.-R. Li and Y.-K. Li, *PLoS One*, 2016, **11**, e0155905.
2 J. D. Fuller and D. E. Low, *Clin. Infect. Dis.*, 2005, **41**, 118–121.
3 C. Y. Chang, B. R. Li and Y. K. Li, *Int. J. Antimicrob. Agents*, 2016, **47**, 416–418.
4 Y. Z. Zhang, D. J. Isaacman, R. M. Wadowsky, J. Rydquistwhite, J. C. Post and G. D. Ehrlich, *J. Clin. Microbiol.*, 1995, **33**, 596–601.
5 F. Gutiérrez, M. Mar, J. C. Rodríguez, A. Ayelo, B. Soldán, L. Cebrián, C. Mirete, G. Royo and A. M. Hidalgo, *Clin. Infect. Dis.*, 2003, **36**, 286–292.
6 J. C. Moïsi, S. K. Saha, A. G. Falade, B.-M. Njanpop-Lafourcade, J. Oundo, A. K. M. Zaidi, S. Afroj, R. A. Bakare, J. K. Buss, R. Lasi, J. Mueller, A. A. Odekanmi, L. Sangaré, J. A. G. Scott, M. Deloria Knoll, O. S. Levine and B. D. Gessner, *Clin. Infect. Dis.*, 2009, **48**, S49–S56.
7 C.-T. Lin, S.-H. Kuo, P.-H. Lin, P.-H. Chiang, W.-H. Lin, C.-H. Chang, P.-H. Tsou and B.-R. Li, *Sens. Actuators, B*, 2020, **316**, 128003.
8 P.-H. Lin, W.-L. Chang, S.-C. Sheu and B.-R. Li, *Iscience*, 2020, **23**, 101658.
9 P.-H. Chang, C.-C. Weng, B.-R. Li and Y.-K. Li, *Biosens. Bioelectron.*, 2020, **151**, 111969.
10 P. H. Lin and B. R. Li, *Analyst*, 2020, **145**, 1110–1120.
11 J. K. Jung, K. K. Alam, M. S. Verosloff, D. A. Capdevila, M. Desmau, P. R. Clauer, J. W. Lee, P. Q. Nguyen, P. A. Pastén, S. J. Matiasek, J.-F. Gaillard, D. P. Giedroc, J. J. Collins and J. B. Lucks, *Nat. Biotechnol.*, 2020, **38**, 1451–1459.
12 P. J. Teoh and A. Maheshwari, *Int. J. Women's Health*, 2014, **6**, 817–827.
13 J. Balsam, M. Ossandon, H. A. Bruck, I. Lubensky and A. Rasooly, *Expert Opin. Med. Diagn.*, 2013, **7**, 243–255.
14 A. La Marca, M. Capuzzo, T. Paglia, L. Roli, T. Trenti and S. M. Nelson, *Reprod. BioMed. Online*, 2020, **41**, 483–499.
15 T. Takazawa, V. Sabato and D. G. Ebo, *Br. J. Anaesth.*, 2019, **123**, e117–e125.
16 B. R. Li, Y. J. Hsieh, Y. X. Chen, Y. T. Chung, C. Y. Pan and Y. T. Chen, *J. Am. Chem. Soc.*, 2013, **135**, 16034–16037.
17 J. B. Haun, T. J. Yoon, H. Lee and R. Weissleder, *Wiley Interdiscip. Rev.: Nanomed. Nanobiotechnol.*, 2010, **2**, 291–304.
18 T. A. P. Rocha-Santos, *TrAC, Trends Anal. Chem.*, 2014, **62**, 28–36.
19 D. M. Bruls, T. H. Evers, J. A. H. Kahlman, P. J. W. van Lankvelt, M. Ovsyanko, E. G. M. Pelssers, J. J. H. B. Schleipen, F. K. de Theije, C. A. Verschuren, T. van der Wijk, J. B. A. van Zon, W. U. Dittmer, A. H. J. Immink, J. H. Nieuwenhuis and M. W. J. Prins, *Lab Chip*, 2009, **9**, 3504–3510.
20 Z. Yang, X. Zou, P. Feng, H. Zhan, D. Xiong and J. Lang, *Inflammation*, 2019, **42**, 1741–1753.
21 D. Pavliakova, P. C. Giardina, S. Moghazeh, S. Sebastian, M. Koster, V. Pavliak, A. McKeen, R. French, K. U. Jansen and M. Pride, *mSphere*, 2018, **3**, e00128-18.
22 E. Ramos-Sevillano, G. Ercoli and J. S. Brown, *Front. Immunol.*, 2019, **10**, 358.
23 S. T. Wu, C. C. Weng, B. R. Li and C. S. Hsu, *J. Mater. Sci.*, 2019, **54**, 10179–10190.
24 S.-T. Wu, C.-Y. Huang, C.-C. Weng, C.-C. Chang, B.-R. Li and C.-S. Hsu, *ACS Omega*, 2019, **4**, 16292–16299.
25 Y.-L. Hsieh, C.-W. Chen, W.-H. Lin and B.-R. Li, *ACS Appl. Bio Mater.*, 2020, **3**, 3304–3312.